journal

J. Am. Ceram. Soc., 89 [7] 2063–2072 (2006)
DOI: 10.1111/j.1551-2916.2006.01025.x

Microwave Dielectric Ceramics for Resonators and Filters in Mobile Phone Networks

Ian M. Reaney[†]

Department of Engineering Materials, University of Sheffield, Sheffield, S1 3JD, U.K.

David Iddles

Filtronic Comtek Enterprise Drive, Wolverhampton, South Staffordshire WV10 7DB, U.K.

Temperature-stable, medium-permittivity dielectric ceramics have been used as resonators in filters for microwave (MW) communications for several decades. The growth of the mobile phone market in the 1990s led to extensive research and development in this area. The main driving forces were the greater utilization of available bandwidth, that necessitates extremely low dielectric loss (high-quality factor), an increase in permittivity so that smaller components could be fabricated, and, as ever in the commercial world, cost reduction. Over the last decade, a clear picture has emerged of the principal factors, that influence MW properties. This article reviews these basic principles and gives examples of where they have been used to control microwave properties and ultimately develop new materials.

I. Introduction

Mobile phone networks allow communication from cell to cell via antennas located on masts and associated base stations. Within a cellular network, the average base station coverage is a diameter of 35 and 18 km at 900 and 1800 MHz, respectively. Each base station houses microwave (MW) resonators that are used to carry signals of a specific frequency and remove (filter) spurious signals and sidebands, that interfere with the quality of the transmitted/received frequency band.

Where selectivity to that frequency is paramount, e.g. narrow bandwidth applications, low loss, temperature-stable ceramics are utilized in preference to cheaper metal cavities.[1] Ceramic pucks suitable for single mode resonator applications are cylindrical and based on the original concepts of Richtmyer,[2] first published in the 1930s. The interaction of the electric and magnetic field lines of electromagnetic (EM) radiation with such a puck is shown in Fig. 1. The puck is designed to sustain a standing wave within its body of a specific resonant frequency and may therefore act as either a filter or a transmitting resonator.[2]

D. Green—contributing editor

Manuscript No. 21257. Received December 16, 2005; approved February 9, 2006.
[†]Author to whom correspondence should be addressed. e-mail: i.m.reaney@sheffield.ac.uk

Along with issues relating to dielectric loss, the cost of a component has become a prime motivator in research and development.

Ceramic resonators are simple in concept but controlling their dimensions and precise phase assemblage during processing is difficult. Any slight differences from batch to batch or within a batch may alter their resonant frequency and temperature stability. Ceramic resonators of differing geometries are shown in Fig. 2, in which single mode pucks are indicated. Multimode resonators are also manufactured, often with unusual geometries to induce several resonant MW modes within their body at any one time. In service, the ceramic conventionally rests within a silver-coated square cavity, as illustrated in Fig. 3. Typically, many hundreds of these cavities will reside in the base stations of a cellular network.

II. Basic MW Properties

For a ceramic to be usable as a dielectric resonator/filter, three key properties need to be optimized[1]; permittivity, $20 < \varepsilon_r < 50$, the temperature coefficient of the resonant frequency, $\tau_f \sim \pm 3$ MK^{-1}, and dielectric loss or rather its inverse, the quality factor, $Q > 30\,000$ at 1 GHz.[1] The permittivity is related to the resonant frequency, f_0, by the following equations;

$$f_0 \approx \frac{c}{\lambda_d \varepsilon_r^{1/2}} \approx \frac{c}{D\varepsilon_r^{1/2}}$$

where c is the speed of light in a vacuum and λ_d is the wavelength of the standing wave along the diameter (D) of a resonator. Consequently, if the permittivity is increased, the size of the resonator may be decreased while still maintaining a specific resonant frequency, i.e. larger permittivities enable miniaturization.

The quality factor, Q, is approximately equal to $1/\tan\delta$. However, this definition is not particularly useful for visualizing how Q relates to microwave communications. More succinctly, it is determined as the resonant frequency (f_0) divided by the bandwidth, Δf_0, measured at 3 dB below the maximum height at resonance, Fig. 4.[1]

Using this definition, it becomes apparent that Q is a measure of the selectivity of a resonator to a given frequency. Higher Q

Feature

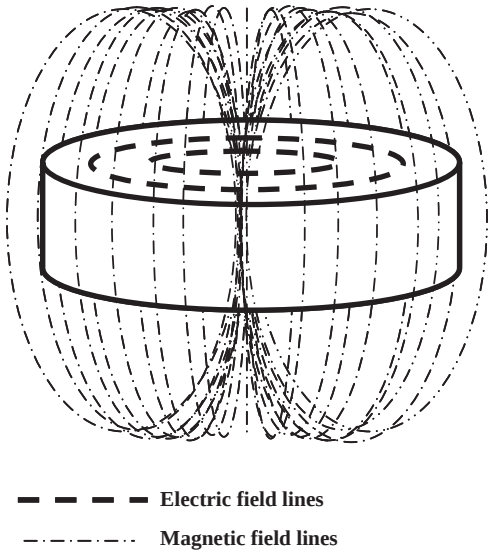

Fig. 1. Interaction of the electric and magnetic field lines with a cylindrical ceramic resonator, after Richtmyer.[2]

values reduce the risk of cross-talk within a given frequency range. Q decreases with increasing frequency and the theoretical relationship between the two is such that $Q \times f_0$ should be constant for any given material, and, often, $Q \times f_0$ values are quoted when comparing ceramics.[1] In practice, however, samples measured at higher frequencies, e.g., 5–10 GHz, always give higher $Q \times f_0$ values than identical materials measured between 1 and 3 GHz. The precise reasons for this are not well understood but may be related to processing. Larger parts, which resonate at lower frequencies statistically contain more flaws and defects than smaller ceramic bodies. $Q \times f_0$ values measured at 1–3 GHz are more relevant, however, representing how the material may perform in a real MW circuit.

τ_f is a measure of the "drift" with respect to the temperature of the resonant frequency. It is self-evident that a material with a significantly non-zero τ_f is useless in an MW circuit (most resonator applications require $\tau_f < \pm 2$ MK^{-1}) as it cannot maintain its resonant frequency as the base station operating temperature changes.[1] τ_f is defined as

$$\tau_f = -(1/2\tau_\varepsilon + \alpha_L)$$

where τ_ε is the temperature coefficient of permittivity and α_L is the linear expansion coefficient. It is related to the temperature coefficient of capacitance (τ_c) by [1]

$$\tau_f = -1/2(\tau_c + \alpha_L)$$

In reality, a small non-zero value of τ_f is required to compensate for thermal expansion of the MW cavity.

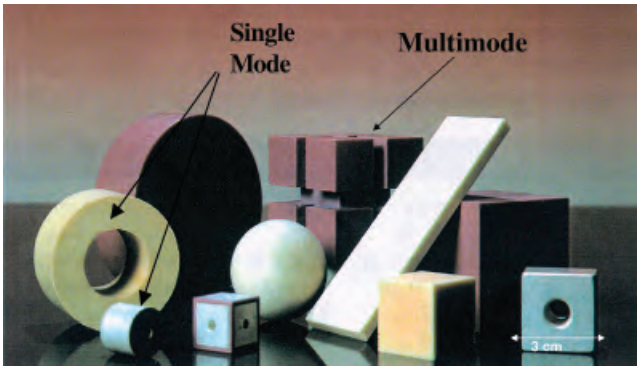

Fig. 2. Various geometries of ceramic puck used as single and multimode resonators and filters.

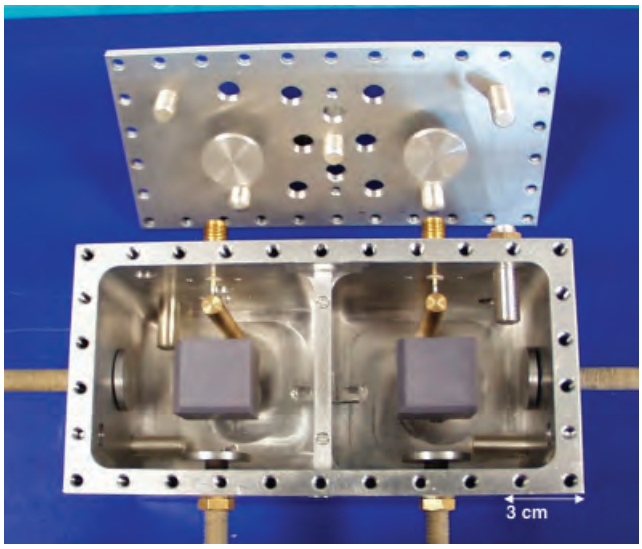

Fig. 3. Silver-coated cavity with pucks used in filter and resonator technology.

In general, microwave dielectric properties are influenced by a number of factors, such as permittivity,[3] onset of phase transitions,[4,5] processing conditions and raw material impurities,[6,7] and order/disorder behavior.[8–11] The following section reviews the types of materials used and factors that control their properties.

III. Microwave Materials

(1) Historical Development

Before discussing specific materials, it is worthwhile reviewing the development and requirements of materials simply from the point of view of MW properties. In doing so, a "roadmap" to the present day is created that illustrates the progression of MW ceramic technology over the last decade, Fig. 5.

In the earliest days of mobile technology, invar air cavities were used as resonators and filters for both base stations and hand sets. These were large and bulky and, in the 1980s, were replaced by the first generation of ceramic resonators based on $(Mg,Ca)TiO_3$, $ZrTiO_4$, and $BaTi_4O_9$. At the start of the 1990s, the ceramic technology for hand sets and base stations diverged. For reasons discussed previously, base stations required higher Q ceramics, $40\,000 < Q \times f_0 < 250\,000$, with materials of relative permittivity $50 > \varepsilon_r > 25$. In contrast, ceramic technology in hand sets was driven by miniaturization, and negative–positive zero (NP0) chips, $70 < \varepsilon_r < 120$, were utilized, in which Q was dominated not by the ceramic but by the metallization. However, even this class of materials has now been replaced by filters

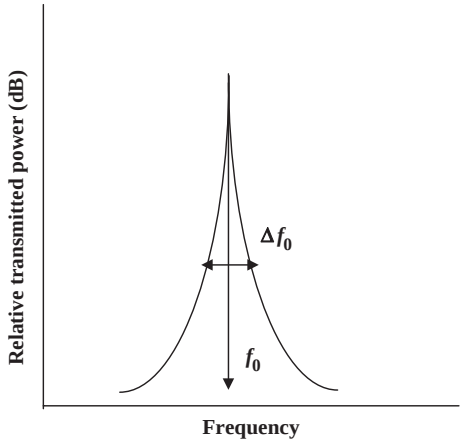

Fig. 4. Schematic showing a resonant peak and associated parameters.

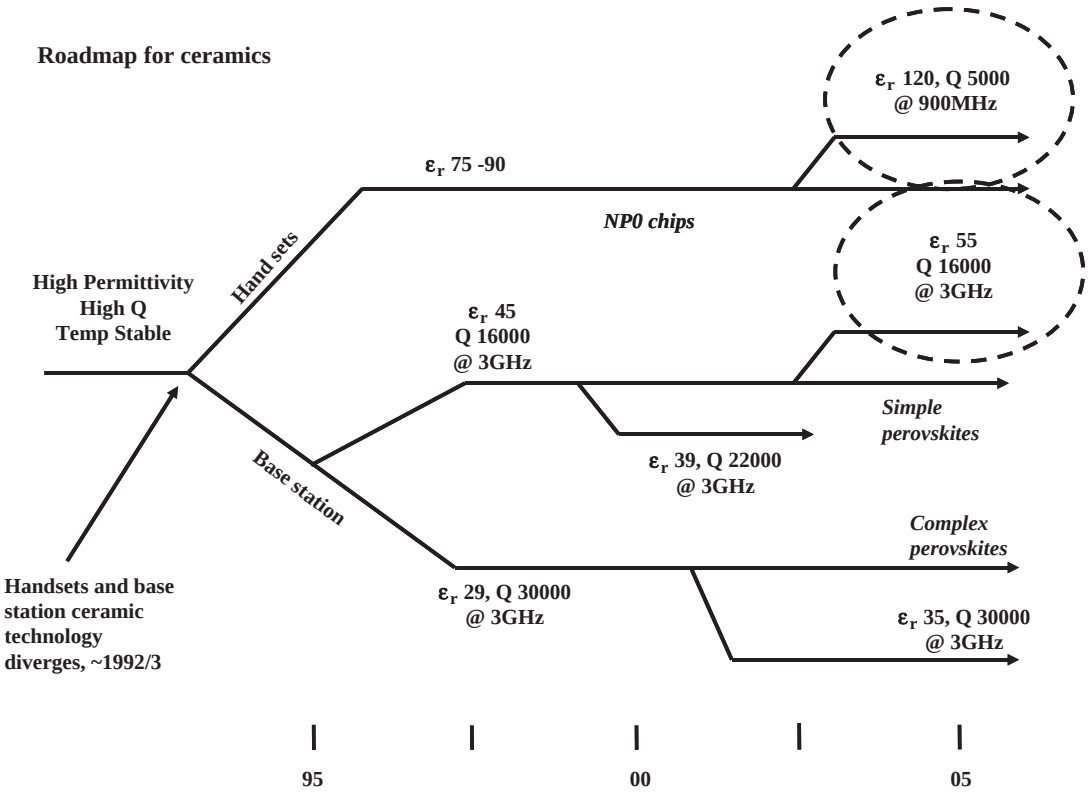

Fig. 5. Road map for ceramics over the last decade. Future requirements for base station ceramics and NP0 chips are ringed.

based on surface acoustic wave (SAW) and bulk acoustic wave (BAW) technology, which are beyond the scope of this article. Table I shows all current ceramics used as MW resonators in base stations. The only exceptions are $Ba_4Nd_{9.33}Ti_{18}O_{54}$ (BNT)-based compounds, that are used primarily as materials for digital television receivers. $CaTiO_3$–$NdAlO_3$ (CTNA) and $ZrTiO_4$–$ZnNb_2O_6$ (ZTZN)-based ceramics dominate the base station resonator market. $Ba(Co,Zn)_{1/3}Nb_{2/3}O_3$ (BCZN)-based ceramics are the most recent development, and effectively are a cheaper replacement for the more expensive $BaZn_{1/3}Ta_{2/3}O_3$ (BZT)-based materials.

Interestingly, if $\log_{10} Q \times f_0$ for these commercial ceramics is plotted against ε_r, a straight line ensues, Fig. 6.,[12] illustrating the fundamental physical principle that dielectric loss and ε_r are not independent variables.[1] It also illustrates a clear gap between 45 and 75 where zero τ_f, high Q ceramics currently do not exist. The maximum predicted $Q \times f_0$ for a material with, e.g. $\varepsilon_r = 55$, in this range is approximately 35 000 GHz. This is considerably lower than the desired $Q \times f_0$ (48 000 GHz) suitable for base station applications and ringed in Fig. 5. It is highly debatable whether further miniaturization of ceramic resonators is possible while maintaining the necessary selectivity to a given frequency. Moreover, higher ε_r materials pose problems in base station cavities as the EM field is effectively retained within the ceramic. Retention of the field prevents coupling between pucks, thereby affecting filter performance, i.e., the filter frequency window is narrowed.

Increasing the permittivity in a ceramic is typically achieved by substitution of a cation of either greater ionic polarizability and/or ionic radius, which decreases the unit cell volume. This principle is typified by, e.g., the $BaZrO_3$–$BaTiO_3$ solid solution in which substitution of Zr by Ti increases the B-site polarizability at the same time as decreasing the unit cell volume, with a commensurate increase in permittivity. The relation between polarizability, unit cell volume and permittivity is well understood and will not be discussed further.

Table I. List of Current Commercial Cavity Resonator MW Ceramics (all Zero τ_f)

Material	Abbreviation	ε_r	$Q \times f_0$ (GHz)	Structure
$BaMg_{1/3}Ta_{2/3}O_3$	(BMT)	24	250 000	Comp. Per.
$BaZn_{1/3}Ta_{2/3}O_3$	(BZT)	29	150 000	Comp. Per.
$Ba(Co,Zn)_{1/3}Nb_{2/3}O_3$	(BCZN)	34	90 000	Comp. Per.
$SrTiO_3$–$LaAlO_3$	(STLA)	39	60 000	Simp. Per
$CaTiO_3$–$NdAlO_3$	(CTNA)	45	48 000	Simp. Per
$ZrTiO_4$–$ZnNb_2O_6$	(ZTZN)	44	48 000	α pbO_2
$Ba_4Nd_{9.333}Tu_{18}O_{54}$	(BNT)	80	10 000	Per/TTB

Comp., complex; Per, perovskite; Simp., simple; TTB, tetragonal tungsten bronze; MW, microwave.

(2) *Factors Affecting* τ_f

(A) Permittivity: In the late 1960s, Harrop[3] compared τ_c with ε_r of paraelectric materials, Fig. 7. Compounds with low ε_r in general exhibit low τ_c and vice versa. Harrop[3] considered the Classius–Mosotti (CM) equation, which relates permittivity, ε,

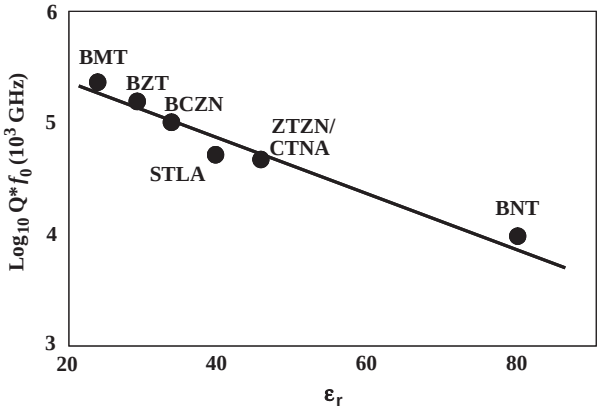

Fig. 6. Graph of $\text{Log}_{10}\ Q \times f_0$ versus ε_r for zero τ_f commercial resonators.[12]

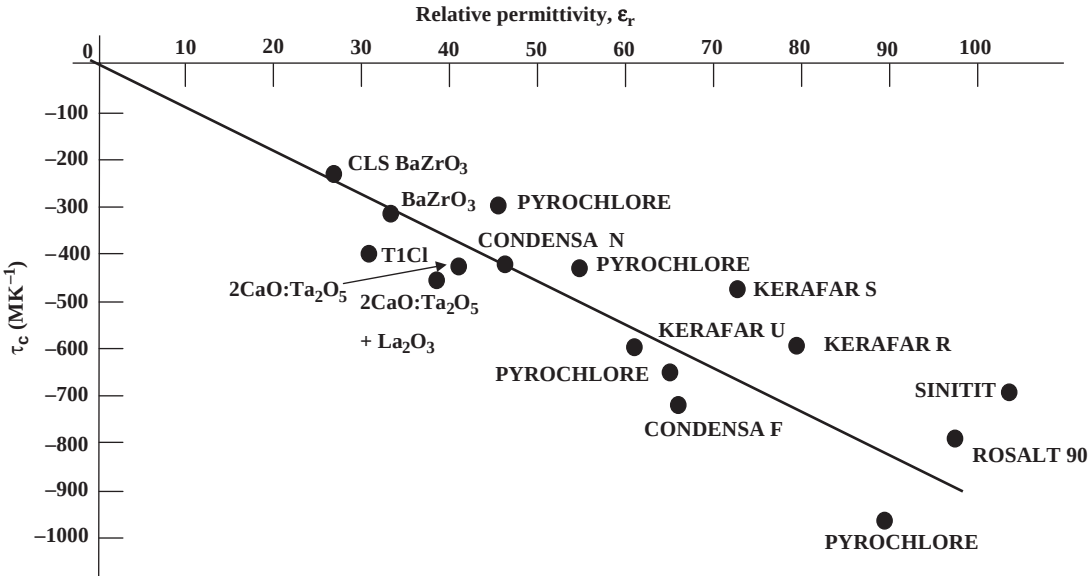

Fig. 7. τ_c versus ε_r for a wide range of materials, after Harrop.[3]

to polarizability, α_j

$$\frac{\varepsilon - 1}{\varepsilon + 2} = \frac{4\pi}{3} \sum N_j \alpha_j$$

where N_j is the concentration of atoms. Harrop[3] differentiated the CM equation to justify physically the following empirical relationship

$$\tau_c = -\alpha_L \varepsilon_r.$$

It follows that

$$\tau_\varepsilon \propto -\alpha \varepsilon_r.$$

As $\tau_f = -(1/2\tau_\varepsilon + \alpha_L)$ (Eq. 4), for small values of α_L or large values of τ_ε, τ_f is also controlled by ε_r. In the case of microwave dielectrics, ionic polarizability dominates ε_r and thus τ_f.[1] Figure 8 illustrates this relationship within the xCaTiO$_3$ (CT)–$(1-x)$LaMg$_{1/2}$Ti$_{1/2}$O$_3$ (LMT) solid solution.[13] This solid solution is formed from two end members with similar structures but widely different permittivities. As the CT ($\varepsilon_r = 165$) concentration increases, τ_f increases. The relationship is linear when $\tau_f \gg \alpha_L$ but deviations occur when the magnitude of τ_f approaches that of α_L. Harrop's[3] approach, however, did not consider how structural phase transitions may affect τ_c and therefore by analogy τ_f and τ_ε. It was not until work by Colla *et al.*[4] and Reaney *et al.*[5] was published that the influence of phase transitions on τ_f became apparent.

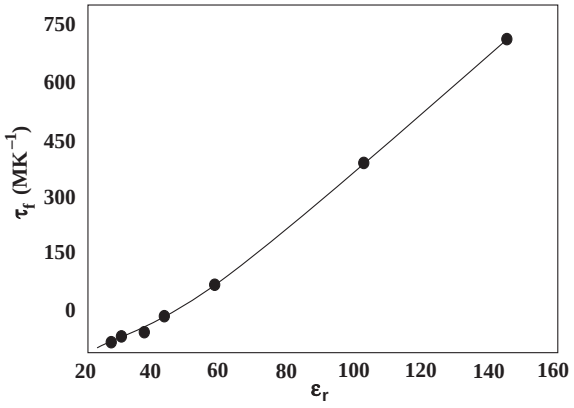

Fig. 8. ε_r versus τ_f for $CaTiO_3$–$LaMg_{1/2}Ti_{1/2}O_3$ solid solutions, after Seabra *et al.*[13]

(3) Phase Transitions

The influence of phase transitions on the microwave properties of Ba- and Sr-based complex perovskites was demonstrated by Colla *et al.*,[4] who showed that a major factor controlling τ_f was the onset of octahedral tilt transitions. Tilt transitions occur when corner-shared O-octahedra rotate either in phase or antiphase around the major axes of the perovskite structure. Sr- and Ba-based complex perovskites typically have $25 < \varepsilon_r < 40$. Therefore, the dependence of τ_f on ε_r is limited. Reaney *et al.*[5] postulated that in perovskites, the tolerance factor,

$$t = \frac{(R_A + R_O)}{\sqrt{2}(R_B + R_O)},$$

where R_A, R_B, and R_O are the radius of the A, B, and O ions, controls the temperature of the onset of octahedral tilt transitions, and therefore τ_f. Lower t's favor distorted structures that have undergone phase transitions on cooling that involve rotations of the O octahedra. The authors pooled previous data and plotted τ_ε versus t for a large number of Sr- and Ba- based complex perovskites, Fig. 9. Three distinct regimes were identi-

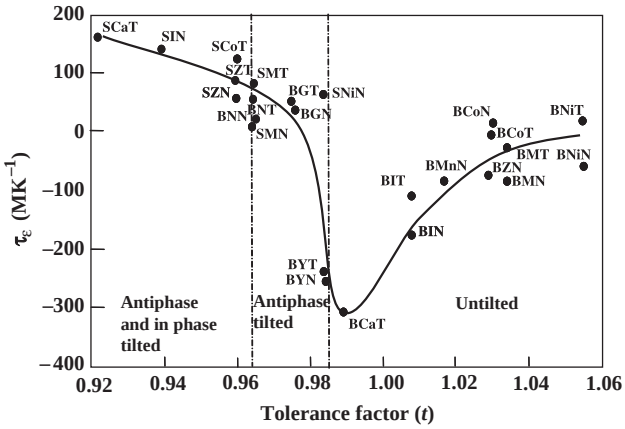

Fig. 9. Tolerance factor, t, versus τ_ε at room temperature for A(B′B″)O$_3$ (A = Sr and Ba, B′ = In, Ca, Mn, Co, Ni, Zn, Mg, Nd, Gd, and B″ = Ta and Nb) 1:1 and 1:2 complex perovskites, after Reaney *et al.*[5]

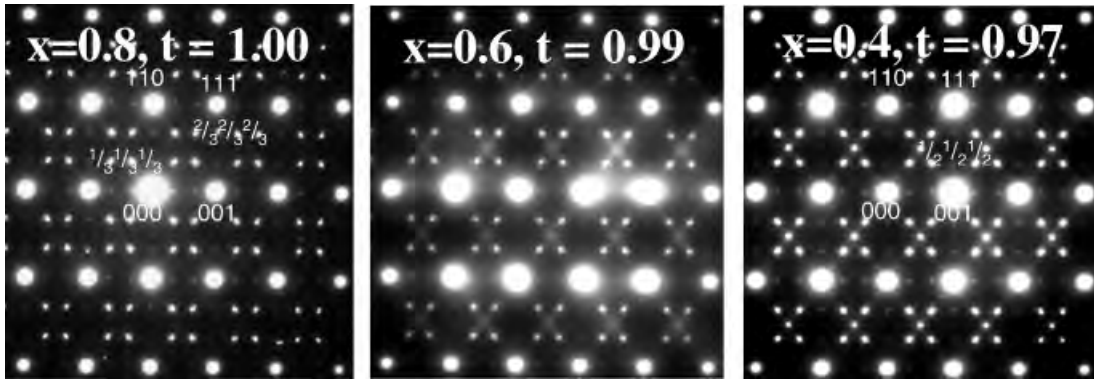

Fig. 10. $\langle 110 \rangle$ zone axis diffraction pattern from grains of $Ba_xSr_{(1-x)}(Zn_{1/3}Ta_{2/3})O_3$ denoting the appearance of reflections as a function of x and t associated with rotations of the O octahedra in antiphase at $1/2\{hkl\}$ or $1/2\{ooo\}$ (where o = odd) positions. Reflections at $\pm 1/3\{hkl\}$ positions arise from ordering of the Zn and Ta ions.

fied by Reaney *et al.*[5] First, for $1.06 > t > 0.985$, τ_ε is initially close to zero but then decreases to a minimum of $-300\ MK^{-1}$ as the tilt transition approaches but does not exceed room temperature. At $t \approx 0.985$, a steep increase in τ_ε occurs, which is associated with the onset of a tilt transition above room temperature in which the octahedra rotate in antiphase only. This phase field persists for $0.985 > t > 0.965$, below which a second phase transition occurs above ambient involving rotations of the octahedra in both antiphase and in phase. In this latter phase field, τ_ε increases as t decreases. It is worth pointing out that t not only controls the onset temperature of a phase transition but also the amplitude of rotation of the octahedra within any given perovskite crystal structure at room temperature.

The onset of octahedral tilting as t decreases is illustrated in Fig. 10, which shows equivalent $\langle 110 \rangle_p$ (where p = pseudocubic) zone axis diffraction patterns from grains in $Ba_xSr_{(1-x)}(Zn_{1/3}Ta_{2/3})O_3$ ceramics. The onset of rotations of the octahedra in antiphase is denoted by the appearance of reflections at $1/2\{hkl\}$ or $1/2\{ooo\}$ (where o = odd) positions. The reflections at $\pm 1/3\ \{hkl\}$ positions arise from ordering of the Zn and Ta ions.

Recently, Lufaso[14] revisited structure property relations in Ba-based complex perovskites and noted that, for 1:2 ordered compounds, neither ε_r nor t correlated well with τ_f for niobates and tantalates. Instead, Lufaso[14] plotted τ_f vs the bond valence sum (BVS) of the B-site M^{2+} ion, Fig. 11. Using this approach, originally outlined by Kucheiko et al.,[15] a strong linear correlation was observed for the six compounds considered. This approach is by no means as universal as considering ε_r and t, both of which apply for a large number of compounds over a broad range of τ_f values. It does, however, illustrate that within narrow groups of similar composition, the degree of underbonding for the B-site M^{2+} ion plays a role in the value and sign of τ_f.

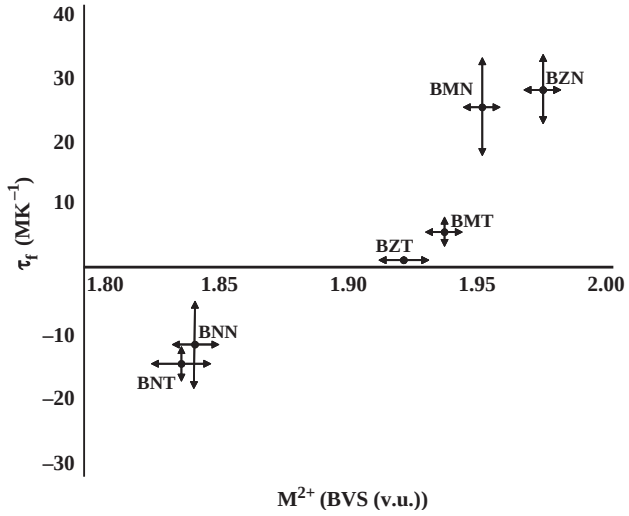

Fig. 11. Average τ_f versus M^{2+} bond valence sum. Error bars represent standard deviation. BNT , $Ba(Ni_{1/3}Ta_{2/3})O_3$; BNN, $Ba(Ni_{1/3}Nb_{2/3})O_3$; BZT, $Ba(Zn_{1/3}Ta_{2/3})O_3$; BMT, $Ba(Mg_{1/3}Ta_{2/3})O_3$; BMN, $Ba(Mg_{1/3}Nb_{2/3})O_3$; BZN, $Ba(Zn_{1/3}Nb_{2/3})O_3$, after Lufaso.[14]

(4) Tuning τ_f

From an engineering perspective, the premise used to obtain a temperature-stable material appears quite simple; a solid solution or composite is created of two materials, each having opposite signs of τ_f. Although this approach adequately explains tuning τ_f from the perspective of a composite, it does not describe the complexities associated with solid solutions.

Within perovskite solid solutions, the true tuning mechanism(s) is/are a combination of the reduction in the polarizability per unit volume (decrease in permittivity)[3] and inducing a phase transition above room temperature usually associated with rotations of the O-octahedra.[4,5] These concepts are schematically illustrated in Fig. 12 for $SrTiO_3$–$LaAlO_3$ solid solutions.[16] $SrTiO_3$ is a high ε_r (290) dielectric that is cubic at room temperature but undergoes a tilt transition to a tetragonal structure ($I4/mcm$) at $\sim -165°C$. $LaAlO_3$ is a low-permittivity (22) dielectric that undergoes an octahedral tilt transition at $\sim 500°C$ to a rhombohedral structure ($R\bar{3}c$) in which the O-octahedra are rotated around the $[111]_p$ direction.[16] As the $LaAlO_3$ concentration increases, the onset temperature of octahedral tilting increases until it is above room temperature. At the same time, the polarizability per unit volume decreases, principally because the long-range coupling of the Ti ions is disrupted by Al^{3+} ions on the B site. The two effects combine to give zero τ_f at a point in the solid solution where $\varepsilon_r = 39$. Figure 13 shows a dark-field image of a commercial zero τ_f $SrTiO_3$–$LaAlO_3$ (STLA) ceramic obtained approximately parallel to a $\langle 110 \rangle_p$ direction using a $1/2\{ooo\}$ reflection.[16] The ribbon-like features are antiphase boundaries arising from regions of tilt that have impinged after

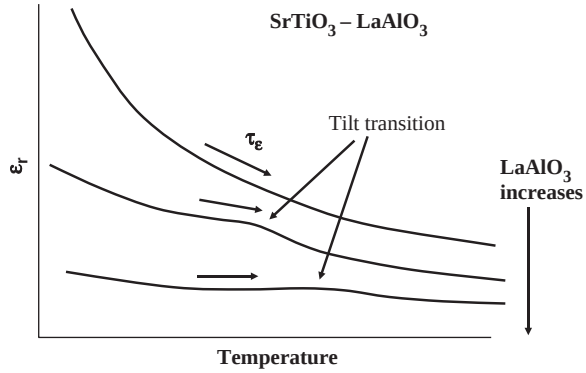

Fig. 12. Schematic showing the tuning mechanisms for tuning τ_ε and therefore τ_f in $SrTiO_3$–$LaAlO_3$. The arrows indicate the qualitative change in τ_ε, after Reaney *et al.*[16]

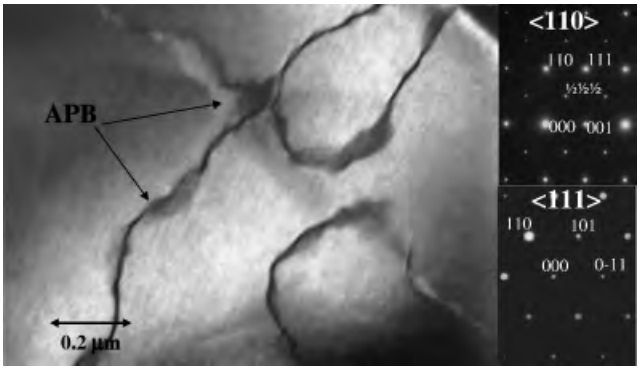

Fig. 13. Dark-field image obtained using a $1/2\{hkl\}$ reflection showing antiphase boundaries (APBs) associated with rotations of the octahedra in antiphase. $\langle 110 \rangle_p$ and $\langle 111 \rangle_p$ zone axis diffraction patterns illustrating that rotations of octahedra occur in antiphase only, after Reaney *et al.*[16]

nucleating out of phase. The absence of superlattice reflections in the $\langle 111 \rangle$ zone axes (Fig. 13) defines the structure as being tilted in antiphase only.[16]

(5) Factors Affecting Q

The optimization of Q is essential to maximize commercial exploitation of the available bandwidths in the 1–3 GHz frequency range. It is the least understood of the three key parameters and is composition, processing, and structure dependent. From a physical perspective, intrinsic losses are controlled by anharmonicity and dampening of the phonon modes of the fundamental lattice[17] and they may be estimated using infra-red spectroscopy in a manner discussed at length by Ferreira *et al.*[18] However, in reality, extrinsic losses dominate Q and optimization usually refers to the minimization of as many extrinsic loss mechanisms as possible.[17] The following sections present an overview of some of the known mechanisms by which extrinsic losses can be minimized.

(A) Order/Disorder Behavior: Some of the most important ordered complex perovskites available commercially are based on doped BZT. Kawashima *et al.*[8] reported the initial MW characterization of BZT for which $\varepsilon_r = 30$, $Q = 6500$ at 12 GHz, and $\tau_f \sim 0$ and also that controlled sintering/annealing of samples led to an improvement in Q. Galasso and Pyle[19] previously reported that BZT is a trigonal perovskite with 1:2 ordering on the B site between Zn and Ta ions along the $[111]_p$ direction. The onset of ordering expands the original unit cell in the $[111]_p$ direction, resulting in the splitting of the $(422)_p$ and $(226)_p$ fundamental perovskite reflections. If Zn and Ta are not ordered, then a cubic structure persists. Kawashima et al.[8] studied the degree of ordering of BZT at various sintering temperatures. Figure 14 shows the splitting of $(422)_p$ and $(226)_p$ peaks with sintering time at 1350°C. At 2 h, there is no lattice distortion (peak splitting), and consequently none or only short-range order (SRO).

After 8 h, the lattice distorts (peak splitting occurs), indicating the onset of long-range B-site ordering. The increase in order is commensurate with an increase in Q to a maximum of 14 000 at 12 GHz. Similar experiments were conducted by Desu and O'Bryan.[20] Tamura *et al.*[21] investigated the BZT system with additions of $BaZrO_3$. They claimed that sintering and crystallization in the $Ba(Zn_{1/3}Ta_{2/3})O_3$–$BaZrO_3$ system were both accelerated by the addition of $BaZrO_3$, and that Q values were improved accordingly. Davies *et al.*[22] further investigated this system and concluded that although at the sintering temperature the addition of <5 mol% $BaZrO_3$ favored face-centered cubic (fcc) order with a random-layer structure, annealing at 1200°C induced 1:2 trigonal, *P3m1*, ordering with a commensurate increase in Q. $BaZrO_3$-doped BZT has $\varepsilon_r = 30$, $Q \times f_0 = 130\,000$ GHz with zero τ_f, and is a commercial system sold by several

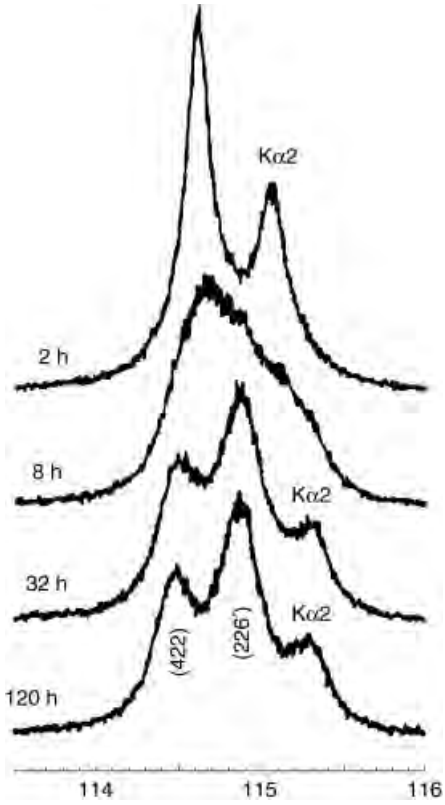

Fig. 14. Splitting of (226) and (422) peaks as a function of sintering time at 1350°C, after Kawashima.[8]

companies. It is a direct competitor with BZT–$SrGa_{1/2}Ta_{1/2}O_3$ (SGT), first investigated by Kageyama *et al.*[23] In two separate studies, Reaney *et al.*[24,25] examined undoped BZT and commercial 0.95BZT–0.05SGT ceramics annealed at various temperatures and used X-ray diffraction and transmission electron microscope to determine the order–disorder transition temperature. For undoped BZT, the order/disorder transition temperature occurred between 1600 and 1625°C.[25] The addition of 5 mol% SGT to BZT results in a decrease in the order/disorder transition to $\sim$1500°C.[24] BZT-based ceramics are sintered at $\sim$1550°C below the order/disorder phase transition for undoped BZT but above that of 0.95BZT–0.05SGT. Consequently, 0.95BZT–0.05SGT requires annealing below the order/disorder transition in order to induce 1:2 ordering, thereby optimizing Q. However, as discussed by Desu and O'Bryan,[20] ZnO loss from the surface of BZT is significant above 1300°C. Therefore, in the study described by Reaney *et al.*,[24] annealing of 0.95BZT–0.05SGT was carried out at 1275°C (below the temperature at which ZnO loss is significant) for 24 h, which resulted in a 40% increase in $Q \times f_0$ from $\sim$110 000 GHz (as sintered) to 150 000 GHz (annealed). Figure 15 shows $\langle 110 \rangle_p$ zone axis diffraction patterns from as-sintered and annealed 0.95BZT–0.05SGT.[25] A dark-field image is included in Fig. 15 obtained using a $\pm 1/3\{hkl\}_p$ reflection which illustrates the microstructure associated with the ordering process.[24] $\langle 110 \rangle_p$ zone axis electron diffraction patterns from the as-sintered ceramics showed diffuse streaks normal to the $\{111\}_p$ planes indicative of SRO, Fig. 15. At the point of crossover, $1/2\{hkl\}_p$ reflections are observed, which have been interpreted as arising from a random-layer, fcc-ordered structure. The diffuse nature of these reflections suggests that this type of ordering is only on the scale length of a few unit cells and in this case may simply be a consequence of 1:2 ordering frustrated by the rapid cooling rate.[24,25]

Upon annealing at 1275°C/24 h, SRO disappears to be replaced by 1:2 trigonal, $P\bar{3}ml$, long-range ordering with discrete reflections at $\pm 1/3\{hkl\}_p$ positions, Fig. 15. These and similar effects have been reported by several authors in BZT-based

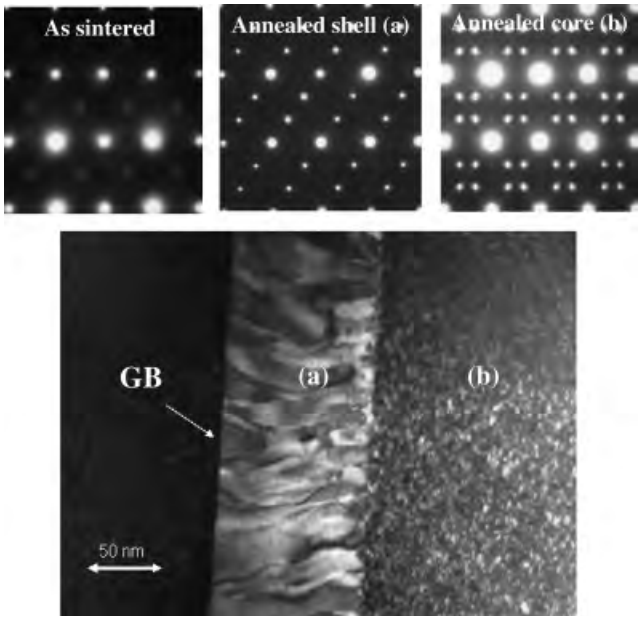

Fig. 15. ⟨110⟩ zone axes from the as-sintered, annealed shell, and annealed core of grains from $0.95BaZn_{1/3}Ta_{2/3}O_3$–$0.05SrGa_{1/2}Ta_{1/2}O_3$. Dark-field image obtained using a $\pm 1/3\{hk\}$ showing the microstructure associated with the ordering. The regions from which two of the electron diffraction patterns are recorded are marked (a) and (b) and GB, grain boundary, after Reaney *et al.*[24]

systems. What is unique in the commercial samples studied by Reaney *et al.*[24] is the magnitude of the resultant $Q \times f_0$ values (150 000 GHz is the largest reported for commercial 2–3 GHz pucks) and the distribution of the ordered domains. A core–shell-ordered microstructure is produced with the shell of every alternate grain composed of a single-ordered, orientational, trigonal variant that contains antiphase boundaries normal to the grain boundary.[24] In contrast, the cores of the grains were composed of multi-variant nano-sized ordered domains, more typical of those previously observed in BZT-based ceramics.[9] In the same study, refinements of neutron and X-ray diffraction data were used to determine the structure of the samples.[24] The data could only be refined assuming a two-phase microstructure in which the average position of the Ta ions differed. The volume fraction of each phase corresponded to approximately that estimated for the core–shell microstructure shown in Fig. 15. The presence of the ordered shell in each alternate grain denotes that this microstructure forms in conjunction with grain growth.[24]

It should be noted that BZT-based ceramics often exhibit a ZnO-deficient phase, $Ba_8ZnTa_6O_{24}$, at their surface. This compound is not significantly detrimental to the properties, as Moussa *et al.*[26] have shown that it has a high Q and permittivity similar to BZT. Attempts to suppress its formation completely by the addition of excess ZnO or firing in a ZnO-rich atmosphere often result in materials with poor Q. The relationship between the presence of this phase at the surface of BZT and higher Q values is not well understood.

(B) Effects of Processing on Q: Negas *et al.*[6] examined the effects of processing on the microwave dielectric properties of $BaTi_4O_9$ and $Ba_2Ti_9O_{20}$ ceramics. They found that raw material impurities (<0.2 wt%) reduced Q by a factor of 2. Minor contamination from milling media and binders degraded Q by 15%–20%. Alford *et al.*[7] studied TiO_2 and observed a maximum of Q for undoped ceramics at 5% porosity. Increasing density degraded Q after that point. This was attributed to coring effects. At a high temperature, titanates are known to undergo partial reduction from Ti^{4+} to Ti^{3+}. This often manifests itself as darkening or coring of the interior of pellets. As the density of the TiO_2 increases, the ingress of O_2 on cooling to reverse the reduction becomes progressively more difficult, which is why Q in undoped TiO_2 has a maximum at densities <100%.

Degradation of Q arises due to the creation of oxygen vacancies (V_O) and possibly the onset of electronic conduction. The formation of vacancies is a plausible explanation from the point of view of phonon–photon interactions and it is intuitively easy to imagine a distribution of V_O increasing the anharmonicity of vibrations and dampening of phonon modes, both of which are classic explanations for extrinsic dielectric loss. A direct link between electronic conductivity and Q is less clear from a mechanistic perspective.

In order to prevent coring, the conventional approach is to process in a high $P(O_2)$ atmosphere or, acceptor dope to inhibit reduction at high temperature. This latter effect was first reported by Herbert,[27] who doped $BaTiO_3$ with Mn oxide to prevent reduction during sintering. A similar approach was used by Alford *et al.*,[7] who doped TiO_2 with Al_2O_3 and improved $Q \times f_0$ dramatically from <6000 to >47 000 GHz. Figure 16 compares the cores of undoped and Al-doped TiO_2 sintered under the same conditions. Undoped TiO_2 shows a complex arrangement of planar defects, whereas Al-doped TiO_2 exhibits a largely featureless microstructure. Planar defects are known to form in TiO_2 when there is a significant reduction.[28]

(C) Effects of Solid Solution on Q: Several MW dielectric ceramics are based on simple (disordered) perovskite solid solutions, in particular, the commercial ceramics, STLA and CTNA.[16] There are a large number of $CaTiO_3$-and $SrTiO_3$-based perovskite solid solutions that form zero τ_f ceramics. However, most compounds, e.g. $(1-x)CaTiO_3$–$(x)Sr(Mg_{1/3}Nb_{2/3})O_3$ (CT-SMN), $(1-x)CaTiO_3$–$(x)Sr(Zn_{1/3}Nb_{2/3})O_3$ (CT-SZN), and CT-LMT, have Q values that are too low for commercial exploitation. The reasons for this are unclear as there are no known issues concerning reduction or unwanted second phases, that could account for this discrepancy. One possible explanation, however, relates to the spread of ionic radius on the A and B sites. This may be rationalized by considering not an average t for a solid solution, as used by Reaney *et al.*[5] in their study of the effect of octahedral tilting on τ_ε, but rather the spread of t (Δt). This approach is similar to that proposed by Attfield and MartinezRodrigues[29] to explain the variations in properties in magnetoresistive manganate-based perovskites. A solid solution is considered to be made up of unit cells of different composition. In CT-SMN, for example, these combinations are as follows: Ca and Ti, Ca and Mg, Ca and Nb, Sr and Ti, Sr and Mg, and Sr and Nb. The t for each of these combinations is calculated and the largest and smallest values are taken to give Δt. In the work quoted below, CT-SMN has a $\Delta t = 0.09$ and $(1-x)CaTiO_3$–$xSr(Zn_{1/3}Nb_{2/3})O_3$ (CT-SZN) has a $\Delta t = 0.1$. In contrast, $CaTiO_3$–$LaGaO_3$ (CTLG) has a low $\Delta t = 0.01$ as Ca^{2+} is similar in size to La^{3+} and Ti^{4+} to Ga^{3+}. Figure 17 shows Δt versus $Q \times f_0$ for several CT-based solid solutions with $40 < \varepsilon_r < 45$ in which a low Δt favors a higher Q, e.g., CTLG has the highest known $Q \times f_0$ values for this class of materials coupled with the lowest Δt. Although Fig. 17 illustrates an empirical relationship, it may be physically justified. A large range of bond lengths on the A and B sites would result in greater anharmonicity and dampening of phonon modes. Moreover, a large Δt would induce a greater driving force for SRO, which would result in nano-clusters of differing bond lengths, further adding to anharmonicity and dampening of the vibrational modes, thereby decreasing Q.

The problem with considering concepts such as clustering and weak SRO effects is determining a means by which they can be detected. In general, such effects are below the detection limit of X-ray and neutron diffraction. Moreover, unless specific cell multiplication phenomena occur, they may also be undetectable by electron diffraction. Vibrational spectroscopy techniques are highly sensitive to SRO and offer a means of detection.[30] Figure 18 shows the Raman spectra between 200 and 1000 wavenumbers for three of the solid solutions described in Fig. 17.[31] The precise assignment of all modes is complex and beyond the scope of this review, but the broad intensities marked as the A_{1g}

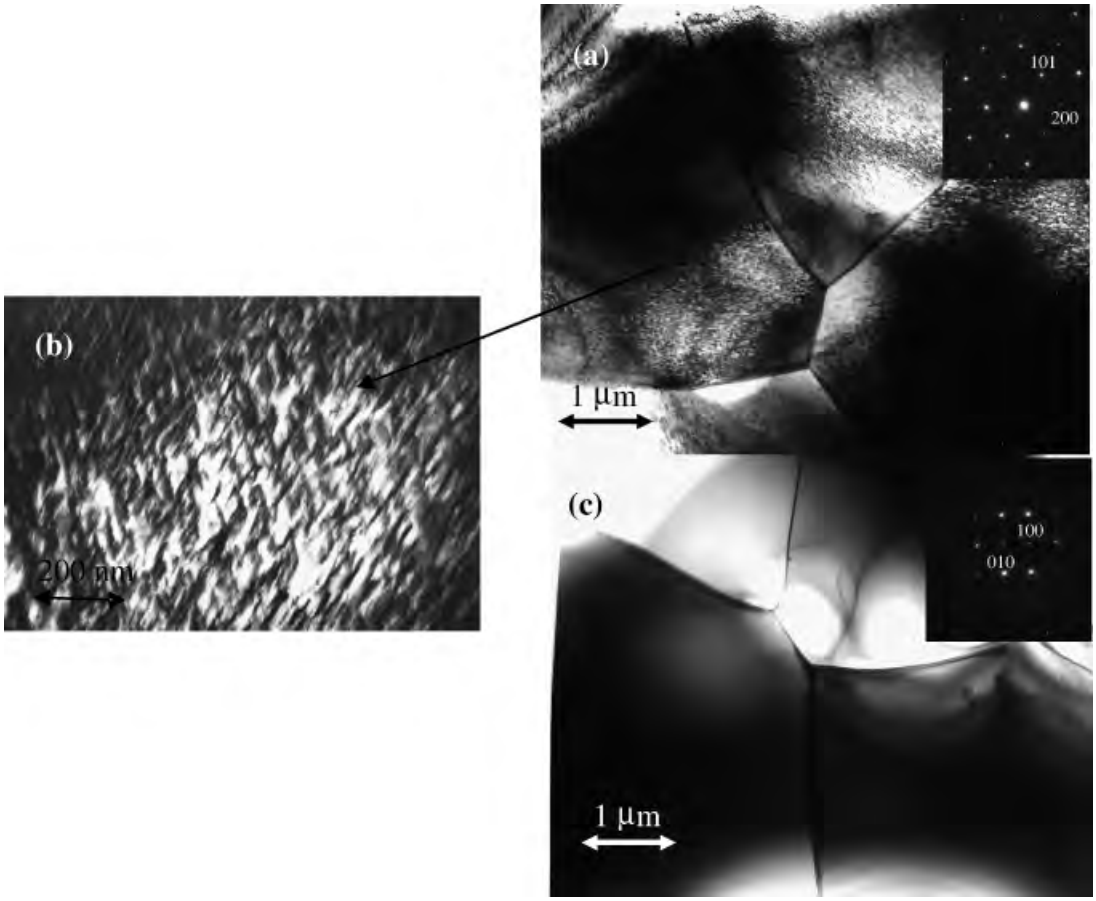

Fig. 16. Bright-field transmission electron microscope images from the core region of (a) and (b) undoped and (c) Al-doped TiO_2.The inset in (a) and (c) show [010] and [001] electron diffraction patterns, respectively. The [010] zone axis shows evidence of superlattice reflections associated with the planar defects.

breathing mode arise because of the presence of more than one B-site ion species. The intensities of Raman spectra is difficult to quantify, particularly when considering so many different ions. However, the full-width at half-maxima (FWHM) of the A_{1g} mode varies considerably, and, the broader this mode for $CaTiO_3$-based solid solutions, the higher the Q. Zheng *et al.*[31] postulated that a broad A_{1g} mode qualitatively indicates only weak SRO and a tendency toward a virtually random distribution of ions on the B site, e.g., CTNA and CTLG. In contrast, zero τ_f CT-SMN has a narrower A_{1g} mode and therefore a greater coherence length of SRO and lower Q.

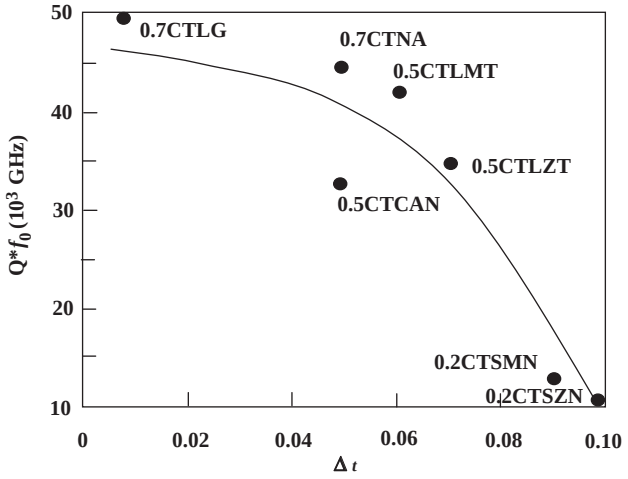

Fig. 17. $Q \times f_0$ versus spread of tolerance factor (Δt) for a range of $CaTiO_3$-based perovskites. $x$$CaTiO_3$ (xCT) $SrMg_{1/3}Nb_{2/3}O_3$ (SMN), $SrMg_{1/3}Zn_{2/3}O_3$ (SZN), $CaAl_{1/2}Nb_{1/2}O_3$ (CAN), $LaMg_{1/2}Ti_{1/2}O_3$ (LMT), $NdAlO_3$ (NA), and $LaGaO_3$ (LG).

For complex perovskites such as BZT, the increase in Q with ordering results in a narrowing of the A_{1g} mode and corresponds to a transition from a short- to long-range-ordered state.[32] It follows therefore that, in complex perovskites, the presence of SRO is detrimental to Q, consistent with the hypothesis presented above for $CaTiO_3$-based solid solutions.

Seabra *et al.*[13] performed a comprehensive study of $x$$BaTiO_3$, $x$$SrTiO_3$, and $x$$CaTiO_3$, in a solid solution with $(1-x)$LMT. Zero τ_f was achieved at $x \sim 0.5$, for all three solid solutions. More interestingly, a minimum in Q in all solid solutions was observed at $x = 0.5$ followed by an increase in Q for $x = 0.7$, Fig. 19. If the concept of nano-clusters discussed above is reasonable, the greatest driving force for their formation must occur at $x = 0.5$, logically accompanied by a minimum in Q (maximum SRO in the solid solution).[13]

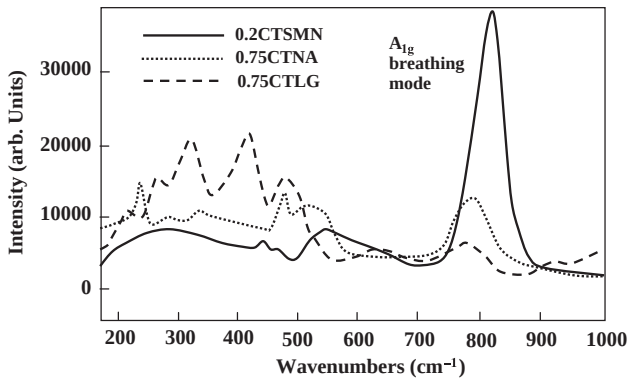

Fig. 18. Raman spectra between 200 and 1000 wavenumbers for three of the solid solutions described in the caption of Fig. 17.

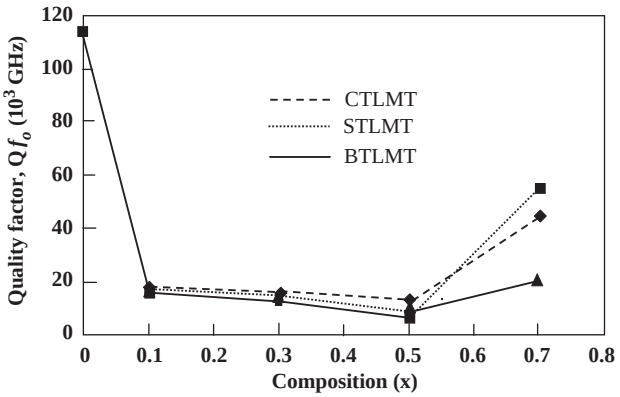

Fig. 19. Q versus x for xCT–$LaMg_{1/2}Ti_{1/2}O_3$ (LMT), xST–LMT, and xBT–LMT solid solutions, after Seabra *et al.*[13]

It may be concluded therefore that with respect to solid solutions, Q is optimized when Δt is a minimum and for zero τ_f compositions that do not fall close to $x = 0.5$. These two factors explain the extraordinarily large $Q \times f_0$ of 0.7CTLG, which Nenasheva[33] has quoted to be as high as 60 000 GHz.

IV. Conclusions

Optimized zero τ_f compositions suitable for resonator applications are rare and only a handful exist. When ε_r is plotted against $\log_{10} Q \times f_0$, all these compositions lie on a straight line. Interestingly, no high Q materials with zero τ_f exist from $45 < \varepsilon_r < 75$. Even if such materials existed, they are not likely to have a Q suitable for base station MW resonator applications.

Factors that control τ_f in MW dielectrics are now well established. A combination of phase transitions, typically involving rotations of the O octahedra, above room temperature and modifying permittivity by adjusting the polarizability per unit volume, are routinely used to control τ_f. Maintaining a high Q while adjusting τ_f is, however, more problematic. Q is highly dependent on processing, and titanates are particularly susceptible to coring and often require firing in high $P(O_2)$ or more cost effectively, acceptor doping to inhibit reduction during sintering at a high temperature. Even when processing is optimized, there are many other factors that influence Q. For complex perovskites, the order/disorder behavior is important. Perovskites that exhibit a trigonal 1:2 ordered cell usually have the highest Q values. To induce ordering, the temperature of the order/disorder phase transition temperature needs to be determined and the sample annealed below this value. ZnO loss can be an issue in, e.g., BZT, so annealing for longer times at reduced temperatures is beneficial.

For $CaTiO_3$ ($\varepsilon_r = 160$)-based solid solutions, Δt needs to be minimized and the zero τ_f composition must avoid $x = 0.5$, so as to minimize the driving force toward SRO. As the permittivity changes as a function of x in accordance with, e.g., the Maxwell mixture rule, avoiding $x = 0.5$ is achieved only if the other end member of the solid solution has $\varepsilon_r < 25$. From this perspective, rare-earth aluminates and gallates are ideal.

In summary, most of the principles that control MW properties in essentially monophase compounds have been empirically demonstrated: tuning τ_f typically requires the following:

(i) manipulation of the permittivity in conjunction with,
(ii) inducing a phase transition above ambient,

for high Q,

(iii) optimize ceramic processing to avoid coring issues, in homogeneity, second phases, impurities, and pressing defects,
(iv) avoid compositions where SRO dominates, and induce LRO if possible (complex perovskites), and
(v) for solid solutions, avoid large differences in ionic radii (mimimize Δt) and utilize end members that induce zero τ_f away from $x = 0.5$.

Many of these simple empirical principles were used to guide the development of $0.9Ba(Co_{0.6}Zn_{0.4})NbO_3$–$0.1BaGa_{1/2}Ta_{1/2}O_3$ (BCZN–BGT) ceramics, that have zero τ_f, $\varepsilon_r = 34$, and $Q \times f_0 > 90\,000$.[34,35] BZN, the base compound in the BCZN–BGT solid solution, has $\tau_f = +20$ MK^{-1}, $Q \times f_0 = 60\,000$ with $\varepsilon_r = 40$.[34] One method of fabricating a zero τ_f resonator using BZN as its base is by doping/forming a solid solution such that the polarizability per unit volume decreases in order to decrease ε_r, thereby tuning τ_ε and τ_f in the manner described originally by Harrop[3] and later by Wise *et al.*[36] Moreover, to maintain a high Q, tuning must be achieved without significantly increasing Δt and also in a manner that retains 1:2 trigonal order. Co^{2+}, when substituting for Zn^{2+}, has a lower polarizability (i.e. decreases permittivity), an ionic radius similar to Nb^{5+} (Δt is therefore unaffected), and it does not disrupt the 1:2 ordering process. BCZN-based ceramics are therefore fabricated.

Undoped BZT has a small negative τ_f (-2 MK^{-1}) and requires tuning by decreasing the average t.[8] Therefore, Kageyama[8] doped BZT ($t = 1.03$) with 5 mol% SGT ($t = 0.96$) to achieve zero τ_f. The addition of SGT had the added advantage of improving Q. It is believed that Ga doping of the B-site facilitates enhanced diffusion and improved sintering but the mechanism is unclear. In contrast, BZN has a large $\tau_f = 20$ MK^{-1} and the addition of SGT further increases the magnitude of the temperature coefficient. Therefore, Hughes *et al.*[34] and Reaney *et al.*[35] prepared a solid solution of BGT rather than SGT with BCZN. The former does not significantly alter the average t or Δt and additionally decreases the permittivity, thereby further tuning τ_f via the mechanism discussed by Harrop[3] and Wise *et al.*[36] A temperature-stable BCZN compound can be fabricated without the addition of BGT, but control over the final properties is difficult to achieve and Q and τ_f can vary dramatically from batch to batch. BCZN–BGT ceramics are now commercially available.

V. Future Requirements

In order for microwave dielectric ceramics to be used in base stations, they must inevitably offer a commercial advantage over competing technologies. In particular, metal cavities offer an alternative to ceramic resonators. Q's are considerably lower ($\sim$6000 GHz) but they are two orders of magnitude cheaper. The high cost of ceramics comes from the often expensive raw materials, e.g., Ta_2O_5 and Nb_2O_5, and the complex manufacturing process necessary to ensure optimum properties. Therefore, ceramics are only used for applications where high Q is paramount. Ironically, most academic researchers pursue high-permittivity (>50), zero τ_f compounds, that offer no real advantage to the base station manufacturer as their values of Q are inevitably too low, the cost is too high, and puck-to-puck coupling is inhibited. Instead, more work is needed on improving Q by developing processing techniques, that minimize extrinsic loss. Many researchers have shown that the use of high-purity chemically derived powders may improve Q but until the cost of such powders is significantly reduced, it is unlikely that they will be used by industry.

Where ceramics offer a distinct advantage over competing technologies is in the use of unusual puck geometries to induce multi-mode resonance, thereby saving space and cost. The design of multimode pucks is still, however, experimental and no clear ideal geometry has emerged, which prohibits spurious resonances. In addition, it is debatable whether they have sufficient mechanical stability to survive the industry standard 7g (gravities) drop test. The unusual design also, lays down new challenges to ceramists to control τ_f, Q, and ε_r during ceramic processing.

In conclusion, the MW ceramic resonator market for base station technology has now matured and industry is focused primarily on cost saving and improving Q. New markets for MW ceramics are, however, constantly emerging such as global positioning systems (many of which utilize dielectric resonator antennas), low-temperature co-fired ceramics for embedded

MW circuitry, tuneable filters, and higher frequency applications for advanced radar technology. As we move inexorably forward in the 21st century, environmental considerations will become increasingly important and MW ceramics will need to be environmentally friendly and recyclable.

Acknowledgments

Dr. Reaney would like to thank the Engineering and Physical Sciences Research Council for its support over the years preceding this article.

References

[1]A. J. Moulson and J. M. Herbert, *Electroceramics*. Chapman & Hall, London, 1990.
[2]R. D. Richtmyer, "Dielectric Resonators," *J. Appl. Phys*., **10**, 391–8 (1939).
[3]P. J. Harrop, "Temperature Coefficients of Capacitance of Solids," *J. Mater. Sci*., **4**, 370–4 (1969).
[4]E. L. Colla, I. M. Reaney, and N. Setter, "Effect of Structural Changes in Complex Perovskites on the Temperature Coefficient of the Relative Permittivity," *J. Appl. Phys*., **74** [5] 3414–25 (1993).
[5]I. M. Reaney, E. L. Colla, and N. Setter, "Dielectric and Structural Characteristics of Ba- and Sr-Based Complex Perovskites as a Function of Tolerance Factor," *Jpn. J. Appl. Phys*., **33** [7A] 3984–90 (1994).
[6]T. Negas, G. Yeager, S. Bell, N. Coates, and I. Minis, "*$BaTi_4O_9/Ba_2Ti_9O_{20}$-Based Ceramics Ressurected for Modern Microwave Applications*," *Am. Ceram. Soc. Bull*., **72**, 80–9 (1993).
[7]A. Templeton, X. Wang, S. J. Penn, S. J. Webb, L. F. Cohen, and N. McN. Alford, "Microwave Dielectric Loss of Titanium Dioxide," *J. Am. Ceram. Soc*., **83** [1] 95–100 (2000).
[8]S. Kawashima, M. Nishida, I. Ueda, and H. Ouchi, "$Ba(Zn_{1/3}Ta_{2/3})O_3$ Ceramics With Low Dielectric Loss at Microwave Frequencies," *J. Am. Ceram. Soc*., **66** [6] 421–3 (1983).
[9]D. J. Barber, K. M. Moulding, and J. I. Zhou, "Structural Order in $Ba(Zn_{1/3}Ta_{2/3})O_3$, $Ba(Zn_{1/3}Nb_{2/3})O_3$ and $Ba(Mg_{1/3}Ta_{2/3})O_3$ Microwave Dielectric Ceramics," *J. Mater. Sci*., **32**, 1531–44 (1997).
[10]M. Onada, J. Kuwata, K. Kaneta, K. Toyama, and S. Nomura, "$Ba(Zn_{1/3}Nb_{2/3})O_3$–$Sr(Zn_{1/3}Nb_{2/3})O_3$ Solid Solution Ceramics with Temperature-Stable High Dielectric Constant and Low Microwave Loss," *Jpn. J. App. Phys*., **21** [12] 1707–10 (1982).
[11]D. A. Sagala and S. Nambu, "Microscopic Calculation of Dielectric Loss at Microwave Frequencies for Complex Perovskite $Ba(Zn_{1/3}Ta_{2/3})O_3$," *J. Am. Ceram. Soc*., **75** [9] 2573–5 (1992).
[12]H. Zheng, I. M. Reaney, D. Muir, T. Price, and D. M. Iddles, "Composite Dielectric Ceramics Based on $BaO–Ln_2O_3–TiO_2$ (Ln = Nd, La)," *Jpn. J. Appl. Phys*., **44** [5A] 3087–90 (2005).
[13]M. P. Seabra, V. M. Ferreira, H. Zheng, and I. M. Reaney, "Structure Property Relations in $La(Mg_{1/2}Ti_{1/2})O_3$-Based Solid Solutions," *J. Appl. Phys*., **97** [3] (2005).
[14]M. W. Lufaso, "Crystal Structure, Modelling, and Dielectric Property Relationships of 2:1 Ordered $Ba_3MMi'_2O_9$ (M = Mg, Ni, Zn; M′ = Nb, Ta) Perovskites," *Chem. Mater*., **16**, 2148–56 (2004).
[15]S. Kucheiko, J. W. Choi, H. J. Kim, S. J. Yoon, and H. J. Jung, "Microwave Characteristics of $(Pb,Ca)(Fe,Nb,Sn)O_3$ Dielectric Materials," *J. Am. Ceram. Soc*., **80** [11] 2937–40 (1997).
[16]I. M. Reaney, P. Wise, R. Ubic, J. Breeze, N. McN. Alford, D. Iddles, D. Cannell, and T. Price, "On the Temperature Coefficient of Resonant Frequency in Microwave Dielectrics," *Philos. Mag*., **81** [2A] 501–10 (2001).
[17]V. L. Gurevich and A. K. Tagantsev, "Intrinsic Dielectric Loss in Crystals," *Adv. Phys*., **40** [6] 719–67 (1991).
[18]V. M. Ferreira, J. L. Baptista, S. Kamba, and J. Petzelt, "Dielectric Spectroscopy of $MgTiO_3$-Based Ceramics in the 10^9–10^{14} Hz Region," *J. Mater. Sci*., **28** [21] 5894–900 (1993).
[19]F. Galasso and J. Pyle, "Ordering in Compounds of the $A(B_{0.33}Ta_{0.67})O_3$ Type," *Inorg. Chem*., **2** [3] 482–4 (1963).
[20]S. B. Desu and H. M. O'Bryan, "Microwave Loss Quality of $Ba(Zn_{1/3}Ta_{2/3})O_3$ Ceramics," *J. Am. Ceram. Soc*., **68** [10] 546–51 (1985).
[21]H. Tamura, T. Konoike, Y. Sakabe, and K. Wakino, "Improved High-*Q* Dielectric Resonator with Complex Perovskite Structure," *J. Am. Ceram. Soc*., **67**, C59–C61 (1984).
[22]P. K. Davies and J. Tong, "Effect of Ordering-Induced Domain Boundaries on Low-Loss $Ba(Zn_{1/3}Ta_{2/3})O_3$–$BaZrO_3$ Perovskite Microwave Dielectrics," *J. Am. Ceram. Soc*., **80** [7] 1727–40 (1997).
[23]K. Kageyama, "Crystal Structure and Microwave Dielectric Properties of $Ba(Zn_{1/3}Ta_{2/3})O_3$–$(Sr,Ba)(Ga_{1/2}Ta_{1/2})O_3$ Ceramic," *J. Am. Ceram. Soc*., **75** [7] 1767–71 (1992).
[24]I. M. Reaney, P. L. Wise, I. Qazi, C. A. Miller, T. J. Price, D. S. Cannell, D. M. Iddles, M. J. Rosseinsky, S. M. Moussa, M. Bieringer, and L. D. Noailles, "Ordering and Quality Factor in 0.95 $BaZn_{1/3}Ta_{2/3}O_3$-0.05$SrGa_{1/2}Ta_{1/2}O_3$ Production Resonators," *J. Eur. Ceram. Soc*., **23** [16] 3021–34 (2003).
[25]I. M. Reaney, I. Qazi, and W. E. Lee, "Order—Disorder Behaviour in $Ba(Zn_{1/3}Ta_{2/3})O_3$," *J. Appl. Phys*., **88** [11] 6708–14 (2000).
[26]S. M. Moussa, J. B. Claridge, M. J. Rosseinsky, S. Clarke, R. M. Ibberson, T. Price, D. M. Iddles, and D. C. Sinclair, "$Ba_8ZnTa_6O_{24}$: A High-*Q* Microwave Dielectric from a Potentially Diverse Homologous Series," *Appl. Phys. Lett*., **82** [25] 4537–9 (2003).
[27]J. M. Herbert, *Ceramic Dielectrics and Capacitors*. Gordon and Breach, London, 1985.
[28]R. J. D. Tilley, *Defect Chemistry and its Applications*. Blackie, Glasgow, 1986.
[29]L. M. Rodriguez Martinez and J. P. Attfield, "Cation Disorder and Size Effects in Magnetoresistive Manganese Oxide Perovskites," *Phys. Rev. B*, **54** [22] 15622–5 (1996).
[30]I. M. Reaney, J. Petzelt, V. V. Voitsekhovskii, F. Chu, and N. Setter, "B-Site Order and Infrared Reflectivity in $A(B'B'')O_3$ Complex Perovskite Ceramics," *J. App. Phys*., **76** [4] 2086–92 (1994).
[31]H. Zheng, I. M. Reaney, G. D. Györgyfalva, R. Ubic, J. Yarwood, M. P. Seabra, and V. M. Ferreira, "Raman Spectroscopy of $CaTiO_3$-based Perovskite Solid Solutions," *J. Mater. Res*., **19**, 488 (2004).
[32]S. J. Webb, J. Breeze, R. I. Scott, D. S. Cannell, D. M. Iddles, and N. M. Alford, "Raman Spectroscopic Study of Gallium-Doped $Ba(Zn_{1/3}Ta_{2/3})O_3$," *J. Am. Ceram. Soc*., **85** [7] 1753–6 (2002).
[33]E. A. Nenasheva, L. P. Mudroliubova, and N. F. Kartenko, "Microwave Dielectric Properties of Ceramics Based on $CaTiO_3$–$LnMO_3$ System (Ln–a, Nd; M–Al, Ga)," *J. Eur. Ceram. Soc*., **23** [14] 2443–8 (2003).
[34]H. Hughes, D. M. Iddles, and I. M. Reaney, "Niobate-Based Microwave Dielectrics Suitable for 3rd Generation Mobile Phone Base Stations," *Appl. Phys. Lett*., **79** [18] 2952–4 (2001).
[35]I. M. Reaney, Y. Iqbal, H. Zheng, A. Feteira, H. Hughes, D. Iddles, D. Muir, and T. Price, "Order-Disorder Behaviour in $0.9Ba(Zn_{0.60}Co_{0.40})_{1/3})Nb_{2/3}O_3$–$0.1Ba(Ga_{1/2}Ta_{1/2})O_3$ Microwave Dielectric Resonators," *J. Eur. Ceram. Soc*., **25** [7] 1183–9 (2005).
[36]P. L. Wise, I. M. Reaney, W. E. Lee, D. M. Iddles, D. S. Cannell, and T. J. Price, "Tunability of Tau(f) in Perovskites and Related Compounds," *J. Mater. Res*., **17** [8] 2033–40 (2002).

□

Ian Reaney joined the Department of Engineering Materials at the University of Sheffield, U.K. in 1994, as a post doctoral research assistant (PDRA), then as lecturer, and as a reader since 2001. He attained his Ph.D. from the University of Manchester in 1989 and worked as a PDRA at the University of Essex before joining the group of Prof. Setter at the Laboratoire de Ceramique, Ecole Polytechnique Federale de Lausanne in Switzerland. He is also an adjunct professor at the Department of Materials Science and Engineering, Pennsylvania State University, U.S.A.

The main theme of Dr. Reaney's research is the use of analytical and high-resolution transmission electron microscopy to study structure/microstructure property relations in electroceramics. His research activities are mainly concerned with materials for sensor and actuator applications and dielectrics for microwave communications. He has published almost 200 papers and in 2002 was the joint recipient of the Edward C. Henry award for best paper (electronics division) in the Journal of the American Ceramic Society.

David Iddles is the Development Manager for Filtronic Comtek, Ceramics Division. David is a member of both the American Ceramic Society and the Institute of Materials and a Chartered Engineer. His research interests are in electroceramic materials, particularly Microwave Dielectric Ceramics for application in mobile phone base station filters.